

PCCP

Accepted Manuscript



This is an *Accepted Manuscript*, which has been through the Royal Society of Chemistry peer review process and has been accepted for publication.

Accepted Manuscripts are published online shortly after acceptance, before technical editing, formatting and proof reading. Using this free service, authors can make their results available to the community, in citable form, before we publish the edited article. We will replace this *Accepted Manuscript* with the edited and formatted *Advance Article* as soon as it is available.

You can find more information about *Accepted Manuscripts* in the [Information for Authors](#).

Please note that technical editing may introduce minor changes to the text and/or graphics, which may alter content. The journal's standard [Terms & Conditions](#) and the [Ethical guidelines](#) still apply. In no event shall the Royal Society of Chemistry be held responsible for any errors or omissions in this *Accepted Manuscript* or any consequences arising from the use of any information it contains.

Barium ferrite decorated reduced graphene oxide nanocomposite for effective electromagnetic interference shielding

Meenakshi Verma^a, Avanish Pratap Singh^b, Pradeep Sambyal^b, Bhanu Pratap Singh^c, S. K. Dhawan^b, and Veena Choudhary^{a}*

^a *Centre for Polymer Science & Engineering, Indian Institute of Technology, Hauz Khas,
New Delhi, 110016, India*

^b *Polymeric & Soft Materials Section, CSIR-National Physical Laboratory
Dr. K. S. Krishnan Road, New Delhi, 110 012, India*

^c *Physics and Engineering of Carbon, CSIR-National Physical Laboratory
Dr. K. S. Krishnan Road, New Delhi, 110 012, India*

E-mail: veenach@hotmail.com

Abstract:

There is an increased interest in the development of high performance microwave shielding materials against electromagnetic pollution in recent years. Barium ferrite decorated reduced graphene oxide (BaFe₁₂O₁₉@RGO) nanocomposite was synthesized by high energy ball milling technique and its electromagnetic properties were investigated in the frequency range of 12.4-18 GHz (Ku band). The results showed that barium ferrite (BaFe₁₂O₁₉) nanoparticles with an average particle size of 20–30 nm were well distributed and firmly anchored onto the surface of the reduced graphene oxide sheets. The obtained nanocomposite exhibited a saturation magnetization of 18.1emu/g at room temperature. The presence of BaFe₁₂O₁₉ nanoparticles in the nanocomposite enhances the space charge polarization, natural resonance, multiple scattering and the effective anisotropy energy leading to a high electromagnetic interference shielding effectiveness of 32 dB (~99.9% attenuation) at a critical thickness of 3 mm. The results

suggested that the as-prepared BaFe₁₂O₁₉@RGO nanocomposite showed great potential as an effective candidate for the new type of microwave absorbing materials.

Introduction

The rapid growth of modern electronics equipped with highly integrated circuits has led to a new kind of pollution known as electromagnetic interference (EMI). EMI has emerged as an extremely serious problem affecting the functioning of electronic devices as well as causing harmful effects to the health of human beings. Therefore, shielding is required for protecting electronics associated with the strategic systems such as aircraft, nuclear reactors, transformers, control systems, communication systems, etc. from unavoidable severe electromagnetic radiations.¹ An EMI shield is needed to achieve the attenuation of electromagnetic radiations either by reflection or absorption and could be used to minimize the electromagnetic reflection from metal surfaces such as aircrafts, ships, tanks, electronic equipments and the walls of anechoic chambers through its dielectric or magnetic loss.² For a high performance EMI shield, lightweight and flexibility are two important technical requirements for applications in areas such as aerospace, aircrafts, automobiles, flexible electronics and wearable devices.³ Typically, materials such as metals, different forms of carbon, e.g., graphite and its exotic forms such as flexible graphite, expanded graphite, single or multiwalled carbon nanotubes, carbon fibers, carbon black, reduced graphene oxide (RGO), graphene, conducting polymers, dielectric, magnetic materials and their composites have been widely used as EMI shields due to their high conductivity and good dielectric and magnetic properties.⁴ However, metals have disadvantages like heavy weight, corrosion susceptibility and cumbersome processing methods which made these materials unsuitable for both the researchers and users.⁵ On the other hand, carbon based

composites have gained significant improvement as EMI shielding materials because of their low cost, facile synthesis and ease of processing.^{1, 6-10}

Graphene, a flat monolayer of carbon atoms tightly packed into a two dimensional honeycomb lattice, has acquired tremendous consideration owing to its unique properties such as remarkable structural flexibility, superior electrical conductivity, thermal stability and extraordinary mechanical properties¹¹. Due to its superior in-plane properties, graphene and graphene like nanomaterials are promising candidates for many potential applications in many technological fields such as polymer nanocomposites,¹² supercapacitors,¹³⁻¹⁴ nanoelectronics,¹⁵ energy storage devices,¹⁶ batteries,¹⁷ sensors,¹⁸ and so forth. The excellent electrical properties and high specific surface area make graphene very promising for electromagnetic shields to absorb incident electromagnetic waves.¹¹ In the drive to develop efficient microwave absorbers and electromagnetic shields, graphene and graphene like materials integrated with inorganic nanostructures have received tremendous attention in recent years due to the rapid growth of electronic industry.^{5, 10, 19} Graphene is highly desirable as an electromagnetic wave absorber at high frequencies over the gigahertz range due to its high dielectric loss and low density.²

Barium ferrites ($\text{BaFe}_{12}\text{O}_{19}$) are well known hard magnetic materials which find applications in many fields such as permanent magnets, magnetic recording media, microwave devices and electromagnetic interference shielding.²⁰ Barium ferrite possesses large saturation magnetization, high Curie temperature together with excellent chemical stability and corrosion resistivity.²¹ Among the magnetic nanoparticles, hexagonal ferrites are well known traditional microwave absorbers but the high density and lower dielectric loss restrict their wide applications as microwave absorbers.²² To overcome these shortcomings, dielectric loss fillers such as conducting polymers, carbon nanotubes and graphene are added.²³ Combining the

extraordinary properties of graphene as well as barium ferrite nanoparticles, BaFe₁₂O₁₉@graphene nanocomposites would be very attractive for potential applications such as electromagnetic interference shielding, high frequency microwave absorbing materials and radar devices.

A number of studies on microwave absorption and shielding of ferrite nanoparticles containing conductive nanocomposites have been reported in the literature. Ohlan et al. investigated the electromagnetic properties of poly(3,4-ethylenedioxythiophene)/BaFe₁₂O₁₉ nanocomposite in the Ku band frequency region (12.4-18 GHz) and they reported a maximum shielding effectiveness due to absorption of -22.5 dB at 15 GHz with minimal reflection loss of -2dB.²⁴ In another course of investigation, Ohlan et al. achieved a maximum shielding effectiveness due to absorption of about -12.1 dB in the Ku band region by incorporating barium ferrite during the emulsion polymerization of copolymers of aniline and 3,4-ethylenedioxythiophene as compared to -6.3 dB for copolymer without barium ferrite.²⁵ Conducting polymer nanocomposites of poly(phenyl amine) with barium ferrite nanoparticles exhibit a maximum shielding effectiveness due to absorption of -28.9 dB at 18 GHz.²⁶ Fenfang Xu and coworkers reported a facile in situ polymerization route to synthesize chiral polyaniline (PANI)/barium ferrite composite. Chiral PANI/ BaFe₁₂O₁₉ composite exhibited excellent microwave absorbing properties with the minimum reflection loss of -30.5 dB at 33.25 GHz with a thickness of only 0.9 mm.²⁷ Xu et al. achieved a maximum reflection loss of -11.8 dB at 11.6 GHz by 13.5 wt% barium ferrite nanoparticles loaded polypyrrole composite with a thickness of 2 mm.²⁸

Herein, we report the successful preparation of BaFe₁₂O₁₉ decorated RGO nanocomposite through the high energy ball milling method. The microwave shielding and dielectric properties

of the nanocomposite were studied in the 12.4-18 GHz frequency range and it is observed that the incorporation of $\text{BaFe}_{12}\text{O}_{19}$ significantly contributes towards the enhanced microwave absorbing performance which is due to its high magnetic losses.

Materials

Natural graphite powder (purity 99.5%, particle size $50\mu\text{m}$) was purchased from Loba Chemie, India. Concentrated sulphuric acid (H_2SO_4) (98%), ortho-phosphoric acid ($\text{o-H}_3\text{PO}_4$) (88%), hydrochloric acid (HCl) (37%) and hydrogen peroxide (H_2O_2) (50%) were purchased from Merck, Belgium. Potassium permanganate (KMnO_4) and ethanol were acquired from Fisher Scientific, India. Citric acid (Merck, India), barium nitrate ($\text{Ba}(\text{NO}_3)_2$) and ferric nitrate ($\text{Fe}(\text{NO}_3)_3$) and ammonium hydroxide solution obtained from Qualigens (India) were used as received without further purification.

Synthesis of reduced graphene oxide

Graphene oxide (GO) was synthesized from natural graphite powder using an improved Hummer's method.²⁹ In a typical synthesis, 3g (1 wt. eq.) natural graphite powder was added to the reaction flask containing homogeneous mixture of H_2SO_4 (360ml) and $\text{o-H}_3\text{PO}_4$ (40ml) under vigorous stirring, immersed in an ice bath. After achieving uniform dispersion of graphite powder, 18g (6 wt. eq.) KMnO_4 was added slowly into the reaction flask producing a slight exotherm to $35^\circ\text{-}40^\circ\text{C}$. The slurry formed was then heated to 50°C and stirred for 20 h. The solution was diluted in ice cold DI water (400ml) followed by addition of H_2O_2 (10ml) at room temperature. The mixture was washed repeatedly by centrifugation till pH 7 was attained. To remove the metal ions, HCl was used during centrifugation. The final product was recovered with ethanol and dried at 60°C in a vacuum oven. The dried GO powder was quickly inserted

into a muffle furnace preheated to 1050°C and held in the furnace for 30 sec to form reduced graphene oxide (RGO).

Synthesis of barium ferrite

For the preparation of barium ferrite, $\text{Ba}(\text{NO}_3)_2$, $\text{Fe}(\text{NO}_3)_3$ and citric acid were taken as starting materials. Desired amounts of $\text{Ba}(\text{NO}_3)_2$ and $\text{Fe}(\text{NO}_3)_3$ were dissolved in a minimum amount of distilled water to get a clear solution. The molar ratio of Ba to Fe was kept 1:11.5. An aqueous solution of citric acid was mixed with the nitrate solution (mixture of $\text{Ba}(\text{NO}_3)_2$ and $\text{Fe}(\text{NO}_3)_3$). The molar ratio of citric acid to total moles of nitrate ions was fixed at 1:1. Ammonia solution was slowly added to adjust the pH at 7. Finally the mixed solution was allowed to evaporate to dryness by heating at 100 °C on a hot plate with continuous vigorous stirring. As water evaporated, the solution became viscous and finally formed a very viscous brown gel. With continuous heating on the hot plate and increasing the temperature to about 200 °C, the gel bubbled up and automatically ignited with glowing flints. The auto ignited dried gel was burnt in a self propagating combustion manner until all of it was completely burnt out to form a brown-colored loose powder. The as-burnt powder was calcined at 900 °C for 2h in air to get the barium ferrite phase.²⁵

Synthesis of barium ferrite/reduced graphene oxide nanocomposites

The as-prepared reduced graphene oxide and barium ferrite were used as raw materials for the ball milling. With a ball to powder mass ratio of 10:1, 1.5 g of $\text{BaFe}_{12}\text{O}_{19}$ and 1.5 g of RGO, stainless steel balls ($\Phi=10$ mm) were introduced into a vial mounted on a Retsch “PM-400” high energy planetary ball mill. The mixture was ball milled at 400 rpm at room temperature under air atmosphere for 4 h.

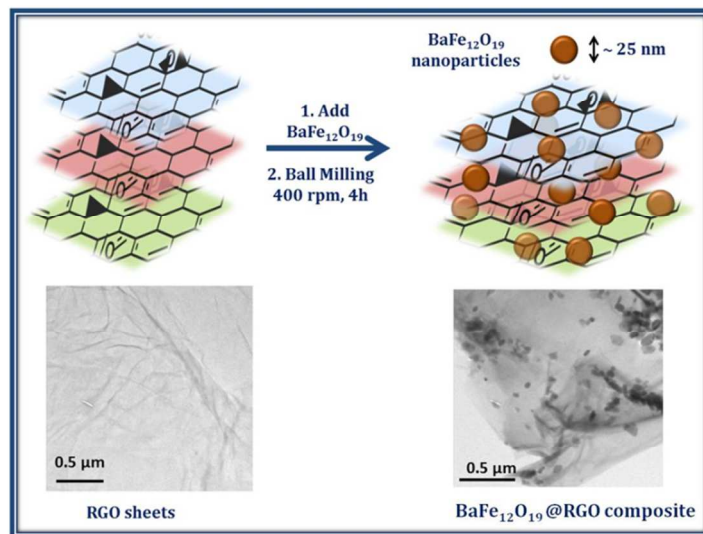


Fig.1 Schematic representation of the preparation of $\text{BaFe}_{12}\text{O}_{19}@RGO$ nanocomposite.

Characterization Techniques

The powder X-ray diffraction (XRD) patterns were recorded on a Bruker D8 Advanced diffractometer employing a scanning rate of $2^\circ/\text{min}$ in a 2θ range from 5° to 70° with $\text{Cu K}\alpha$ radiation ($\lambda=1.5418\text{\AA}$). Thermogravimetric analyzer (Mettler Toledo TGA/SDTA 851e) was used to measure the thermal stability of the composite under inert atmosphere (flowing N_2 gas) in the temperature range 25° - 900°C at a heating rate of $10^\circ\text{C}/\text{min}$. Raman spectra were recorded on a Renishaw inVia reflex Raman spectrometer, UK with an excitation source of 514.5 nm. The resolution of the instrument was less than 1.0 cm^{-1} . Fourier transform infrared spectroscopy (FTIR) analysis was performed at room temperature using a Nicolet 5700 spectrometer in transmission mode in the wave number range 400 - 4000 cm^{-1} . The spectroscopic grade KBr pellets were used for collecting the spectra with a resolution of 4 cm^{-1} , performing 32 scans. The magnetic properties were measured using a vibrating sample magnetometer (VSM) (7304

Lakeshore, USA). The M–H measurements were performed with an applied field range of ± 6000 Oe at room temperature. High resolution transmission electron microscopy (HRTEM) was carried out using a Technai G² F20, USA operating at an accelerating voltage of 300 kV, having a point resolution of 0.2 nm and a lattice resolution of 0.14 nm. TEM specimens were prepared by ultrasonically suspending the powder in ethanol and placing a drop of suspension on a carbon coated copper grid. Scanning electron microscopy (SEM, Zeiss EVO–50) was employed to analyze the morphology of the composite. The S parameters S_{11} (S_{22}), S_{12} (S_{21}) of the barium ferrite decorated reduced graphene oxide composite was measured by vector network analyzer (VNA E8263B Agilent Technologies) in the frequency range of 12.4 – 18 GHz (Ku band) using two port measurement techniques³⁰. The powder samples were compressed into rectangular pellets with dimensions 15.8 X 7.9 mm² and inserted in a copper sample holder connected between the waveguide flanges of a network analyzer. The power coefficients, transmission coefficient (T) and reflection coefficient (R) were calculated by the equations

$$T = \left| \frac{E_T}{E_I} \right|^2 = |S_{21}|^2 = |S_{12}|^2 \quad (1)$$

$$R = \left| \frac{E_R}{E_I} \right|^2 = |S_{11}|^2 = |S_{22}|^2 \quad (2)$$

$$\text{and absorption coefficient was calculated from the relation of } (A) = 1 - R - T \quad (3)$$

Here, it is noted that the absorption coefficient is given with respect to the power of the incident electromagnetic wave. If the effect of multiple reflections between both interfaces of the material is negligible, then the relative intensity of the effectively incident electromagnetic wave inside the material after reflection is based on the quantity $(1 - R)$. Therefore, the effective absorbance (A_{eff}) can be described as $A_{\text{eff}} = A / (1 - R)$ with respect to the power of the effective incident electromagnetic wave inside the shielding material. Absorption efficiency (AE) was obtained using the relation of $AE = A / (1 - R) \times 100\%$. The electromagnetic attributes, dielectric and

permeability parameters have been calculated from the measured S parameters using the Nicolson–Ross–Weir algorithm.³³

Results and Discussion

Morphological Characterization

The surface morphologies of RGO and BaFe₁₂O₁₉@RGO nanocomposite were investigated using SEM. Typical SEM images of RGO and BaFe₁₂O₁₉@RGO nanocomposite are shown in Fig. 2. As can be seen in Fig. 2(a), RGO obtained by the thermal reduction of graphene oxide appeared as a lamellar structure consisting of randomly aggregated sheets. It is clear that BaFe₁₂O₁₉ nanoparticles are assembled on the surface of two dimensional RGO sheets as shown in Fig. 2(b), indicating an electrostatic attraction between RGO and BaFe₁₂O₁₉.

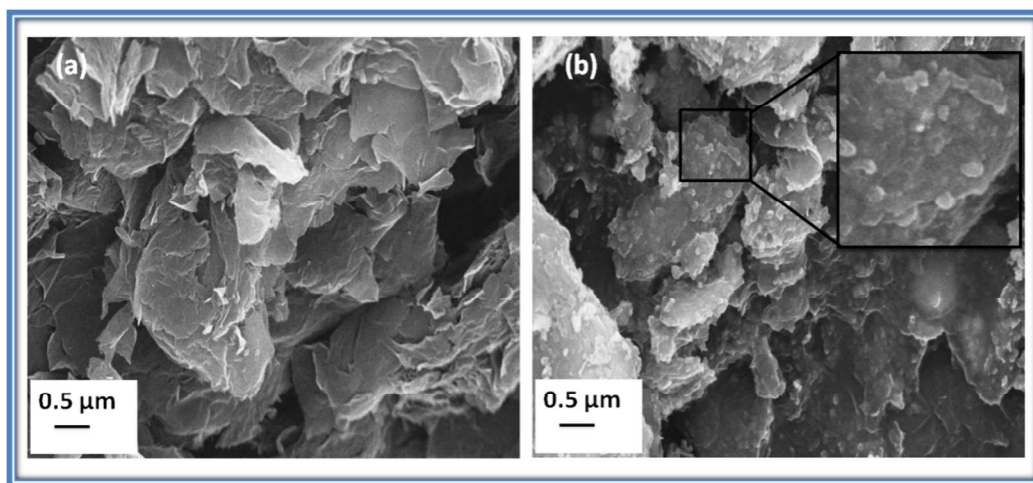


Fig. 2 SEM images of (a) RGO and (b) BaFe₁₂O₁₉@RGO nanocomposite.

Fig. 3 demonstrates TEM and HRTEM micrographs of BaFe₁₂O₁₉, RGO and BaFe₁₂O₁₉@RGO composite. It can be clearly seen in Fig. 3(a) that BaFe₁₂O₁₉ nanoparticles are highly agglomerated with an average particle size in the range of 20-30 nm. Fig. 3(b) show the lattice

plane spacing of the ferrite particles, which is about 0.26 nm corresponding to the (114) plane of $\text{BaFe}_{12}\text{O}_{19}$ phase.²⁴ This is consistent with the results calculated from XRD analysis, Fig. 4 (a). Fig. 3(c) displays an ultrathin, wrinkled paper-like morphology of graphene sheets in RGO. Fig. 3(d) and 3(e) show the TEM images of the $\text{BaFe}_{12}\text{O}_{19}$ @RGO nanocomposite at varying magnification. After ball milling, the original graphene sheets in RGO were crushed into much smaller pieces decorated with nanosized $\text{BaFe}_{12}\text{O}_{19}$. Fig. 3(f) displays a HRTEM image of the composite, where $\text{BaFe}_{12}\text{O}_{19}$ nanoparticle wrapped by the stack of graphene sheets is clearly visible. Beside, these $\text{BaFe}_{12}\text{O}_{19}$ nanoparticles are firmly attached to the graphene sheets of RGO as even after sonication which was used to prepare specimens for TEM images, an excellent adhesion between graphene and $\text{BaFe}_{12}\text{O}_{19}$ nanoparticles was observed.

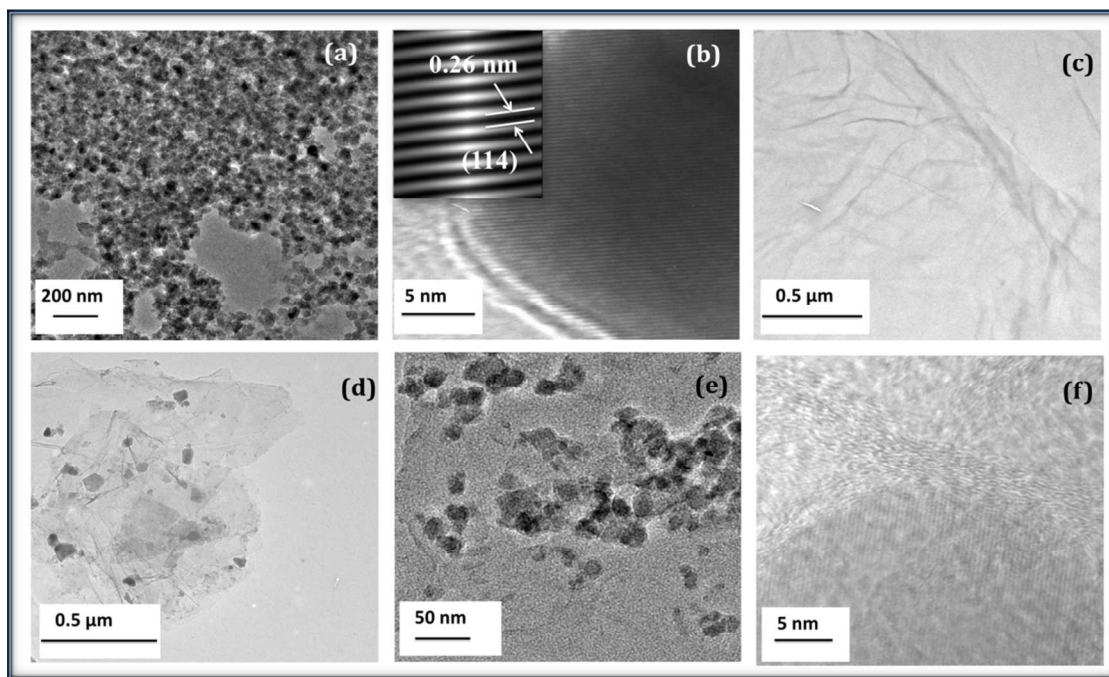


Fig. 3 (a) TEM images of $\text{BaFe}_{12}\text{O}_{19}$ nanoparticles, (b) high magnification HRTEM image of $\text{BaFe}_{12}\text{O}_{19}$ nanoparticles showing the (114) oriented lattice planes of $\text{BaFe}_{12}\text{O}_{19}$, (c) TEM image of RGO sheets, (d) and (e) low and high magnification TEM image of

BaFe₁₂O₁₉@RGO nanocomposite, showing the nanoparticles of BaFe₁₂O₁₉ on the RGO surface and (f) HRTEM image of BaFe₁₂O₁₉@RGO nanocomposite.

Fig. 4(a) presents the XRD profiles of RGO, BaFe₁₂O₁₉ and BaFe₁₂O₁₉@RGO nanocomposite prepared through high energy ball milling method. The characteristic diffraction peak (002) for graphite appears at around $2\theta=26.3^\circ$ indicating that the interlayer distance (d-spacing) between two graphene layers is about 0.334nm. After oxidation, this diffraction peak shifted to a lower angle around $2\theta=12.15^\circ$ corresponding to the (001) plane indicating a highly oxidized sample with increased d spacing of about 0.727nm as shown in Fig. S1 (see supporting information).²⁹ The reduction of GO was confirmed by the absence of the peak at $2\theta=12.15^\circ$ and appearance of broad diffraction peak at $2\theta= \sim 24^\circ$ ascribed to the (002) reflection plane of graphene suggesting that the oxygen functionalities have been removed and GO is effectively reduced to graphene. Main diffraction peaks of barium ferrite were observed at 2θ values of 31.36° ($d = 2.84$), 33.22° ($d = 2.69$), 35.16° ($d = 2.54$), 38.12° ($d = 2.35$), 41.32° ($d = 2.18$), 43.46° ($d = 2.07$), 56.08° ($d = 1.63$), 57.54° ($d = 1.59$) and 64.12° ($d = 1.45\text{\AA}$) corresponding to the (110), (107), (114), (203),(205), (206), (217), (2011) and (220) reflections.²⁴ All the observed peaks of barium ferrite have been matched well with the standard XRD pattern (JCPDS no. 39-1433). The nanocomposite shows the well retained characteristics peaks of BaFe₁₂O₁₉ and no other peak was observed, indicating that no chemical reaction occurred between BaFe₁₂O₁₉ and RGO. However the characteristic peak of RGO at $2\theta = 24^\circ$, due to the (002) plane, was masked by the intense peaks of BaFe₁₂O₁₉ and disappears.

The crystallite size of BaFe₁₂O₁₉ nanoparticles can be calculated by using the Debye-Scherrer formula:

$$D = k\lambda/\beta\cos\theta$$

Where D is the average crystallite size of nanoparticles, k is the shape factor, λ is the X-ray wavelength, θ is the half angle in degrees and β is the full width at half maximum. The value of k is often assigned a value of 0.89, which depends on several factors, including the Miller index of the reflecting plane and the shape of the crystal.³⁴ The (114) reflection of the observed X-ray data was chosen for calculating the crystallite size of BaFe₁₂O₁₉ nanoparticles. The average size of the BaFe₁₂O₁₉ nanoparticles was calculated using the above equation and estimated as 30 nm which is in excellent agreement with the particle size determined by TEM.

Fig. 4(b) demonstrates the FTIR spectra of BaFe₁₂O₁₉, GO, RGO, and BaFe₁₂O₁₉@RGO nanocomposite. The FTIR spectrum of BaFe₁₂O₁₉ shows characteristic peaks at 586, 545, and 431 cm⁻¹ which are due Fe-O bond stretching.²⁴ The characteristics bands of GO were observed at 3432 cm⁻¹ (O-H stretching vibrations), 1720 cm⁻¹ (C=O stretching vibrations from carbonyl and carboxylic acid group), 1150 cm⁻¹ and 1022 cm⁻¹ (C-O stretching vibrations from epoxy and alkoxy group respectively) and 875 cm⁻¹ (C-O asymmetric stretching vibrations from epoxide group).³⁵ The FTIR spectrum of reduced graphene oxide indicates that exfoliation at 1050 °C results in the removal of most of the carboxyl groups and hydroxyl groups. Appearance of new peaks at 2921, 2852, and 1565 due to C-H stretching and C=C stretching vibrations are suggestive of the restoration of the sp² hybridized graphitic structure.³⁶ A slight shift in the main peaks of RGO observed in the FTIR spectrum of BaFe₁₂O₁₉@RGO could be due to some interaction of ferrite particles with the graphene sheets of RGO.²⁴

Thermogravimetric analysis was performed on GO, RGO, BaFe₁₂O₁₉, and BaFe₁₂O₁₉@RGO nanocomposite in nitrogen atmosphere from 25 °C to 850 °C at a heating rate of 10 °C/min (shown in Fig. 4(c)). BaFe₁₂O₁₉, with exceptionally high thermal stability, showed no weight loss over the entire range of temperature. For GO, the mass loss process can be divided into three

stages as: below 150 °C ascribed to the evaporation of adsorbed water, from 150 °C to 400 °C attributed to the removal of the labile oxygen containing functional groups and between 400 °C to 700 °C assigned to the decomposition of more stable oxygen functionalities indicating pyrolysis of the carbon skeleton of the GO.³⁷ In case of RGO, the mass loss is only about 5% up to 300°C because most of the functional groups are removed during reduction leading to the improvement of the thermal stability of the sample. Compared to the curve of RGO, the mass loss of the BaFe₁₂O₁₉@RGO nanocomposite was much lower and tended to be constant up to 575 °C (only 5% weight loss), displaying much higher thermal stability than RGO due to attachment of BaFe₁₂O₁₉ nanoparticles on the RGO sheets.

The magnetization curves of BaFe₁₂O₁₉ and BaFe₁₂O₁₉@RGO nanocomposite measured at room temperature are shown in Fig. 4(d). The saturation magnetization (M_s) value of BaFe₁₂O₁₉ was found to be 40.8 emu/g at an external field of 5kOe. When BaFe₁₂O₁₉ nanoparticles are incorporated in the RGO matrix in 1:1 weight ratio, the M_s value was found to be 18.1 emu/g. The decrease of the saturation magnetization can be attributed to the existence of the non magnetic RGO. The ferrite is shown to be a ferromagnetic phase while RGO is nonmagnetic.

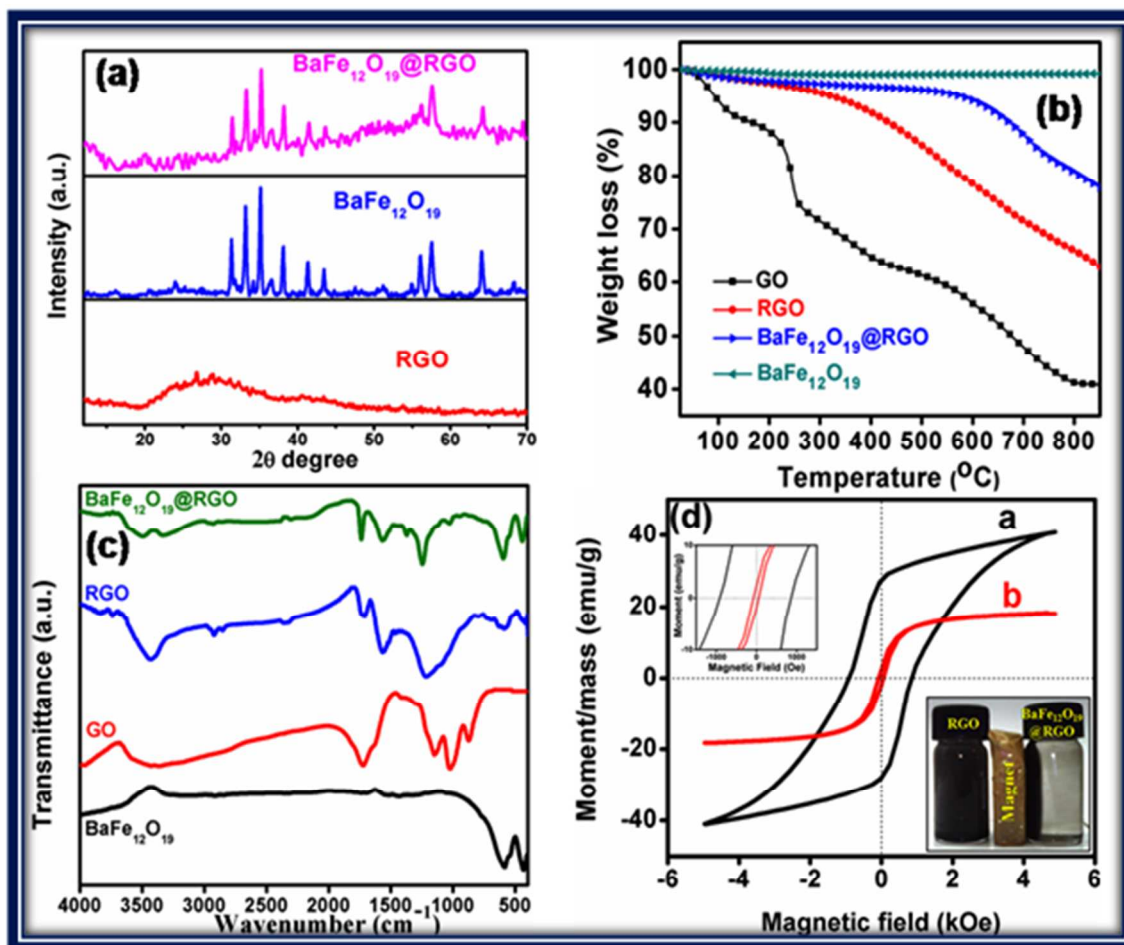


Fig. 4 (a) XRD of RGO, $\text{BaFe}_{12}\text{O}_{19}$ and $\text{BaFe}_{12}\text{O}_{19}@RGO$, (b) thermogravimetric (TG) plots of GO, RGO, $\text{BaFe}_{12}\text{O}_{19}$ and $\text{BaFe}_{12}\text{O}_{19}@RGO$ in N_2 atmosphere, (c) comparison of FTIR spectra of GO, RGO, $\text{BaFe}_{12}\text{O}_{19}$ and $\text{BaFe}_{12}\text{O}_{19}@RGO$ and (d) VSM plots of (a) $\text{BaFe}_{12}\text{O}_{19}$ and (b) $\text{BaFe}_{12}\text{O}_{19}@RGO$.

Raman spectroscopy is an important, powerful and non-destructive tool to characterize carbonaceous materials. Fig. 5 shows the Raman spectra of RGO, $\text{BaFe}_{12}\text{O}_{19}$, and $\text{BaFe}_{12}\text{O}_{19}@RGO$. The characteristic features in the Raman spectra of the graphene like materials are the so-called D band, which locate at around 1350 cm^{-1} , corresponding to the breathing mode of κ -point phonons of A_{1g} , and the G band, in the range of 1500 cm^{-1} to 1600 cm^{-1} , attributed to the tangential stretching mode of the E_{2g} phonons of sp^2 atoms³⁵. Intensity

ratio of D and G band has been used as a measure of the degree of ordered and disordered structures in graphene sheets. On excitation at 514 nm, RGO presented characteristic D and G peaks at 1353 cm^{-1} and 1594 cm^{-1} , respectively, with I_D/I_G ratio of 0.80. The fundamental Raman scattering peaks for $\text{BaFe}_{12}\text{O}_{19}$ observed at 685 cm^{-1} , 614 cm^{-1} , 465 cm^{-1} , 411 cm^{-1} , 317 cm^{-1} are assigned to A_{1g} vibrations of Fe-O bonds at the bipyramidal 2b, octahedral $4f_2$, $2a + 12k$, $12k$ dominated, $2a$ sites respectively. The peaks at 529 cm^{-1} , 292 cm^{-1} , and 211 cm^{-1} are due to E_{1g} vibrations while the peak observed at 336 cm^{-1} is due to E_{2g} vibration modes. The peaks at 183 cm^{-1} and 173 cm^{-1} originates from E_{1g} vibrations of the whole spinel block.³⁸ In addition to the typical peaks of $\text{BaFe}_{12}\text{O}_{19}$ being present in the Raman spectrum of the $\text{BaFe}_{12}\text{O}_{19}@RGO$ nanocomposite, two prominent peaks of the D (1355 cm^{-1}) and G (1597 cm^{-1}) bands from RGO were also observed with an increased intensity ratio I_D/I_G of 0.89. The G band experienced a blue shift of about 3 cm^{-1} compared to RGO with the incorporation of $\text{BaFe}_{12}\text{O}_{19}$. The enhanced intensity ratio I_D/I_G and slight shifting in the bands further support the interaction between $\text{BaFe}_{12}\text{O}_{19}$ nanoparticles and RGO sheets as observed in FTIR.

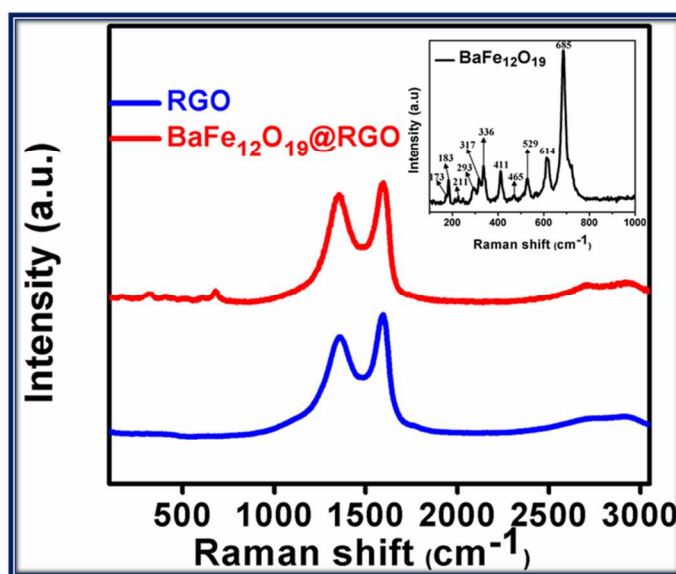


Fig. 5 Raman spectra of RGO and BaFe₁₂O₁₉@RGO. Inset image shows the Raman spectra of BaFe₁₂O₁₉ nanoparticles.

Shielding effectiveness and dielectric measurement

In previous reports, it is well established that moderate conductivity (0.001 - 10 S/cm) is required for improving the microwave absorption and good magnetic properties for enhancing the magnetic losses in the shield³⁹ As can be seen from the results, the barium ferrite decorated reduced graphene oxide composite possesses both characteristics as moderate electrical conductivity (0.98 S/cm) and good magnetic properties. Hence, one would expect that the new, ingeniously synthesized composite could potentially be used in EMI shielding application. Barium ferrite and reduced graphene oxide have been primarily proved for microwave shielding.^{2, 23, 26, 40} Fig. 5 (a) shows the variation of the shielding effectiveness (SE) with frequency in the range of 12.4 –18 GHz (Ku-band).

For a shielding material, total SE = SE_R + SE_A + SE_M,(4)

where SE_R, SE_A and SE_M are shielding effectiveness due to reflection, absorption and multiple reflections, respectively. The EMI SE of a material can be written mathematically as

$$SE(dB) = -10\log\left(\frac{P_T}{P_I}\right) = -20\log\left(\frac{E_T}{E_I}\right) = -20\log\left(\frac{B_T}{B_I}\right) \quad (5)$$

where symbol P, E and B stands for power, electric and magnetic field intensity. The subscript T and I used for the transmitted and incident wave on the shield, respectively. The correction term SE_M can be ignored in all practical applications when SE >10 dB⁴¹, as

$$SE(dB) = SE_R(dB) + SE_A(dB) \quad (6)$$

In equation 6, the first term is related to the reflection of the electromagnetic wave and contributes as the SE due to reflection. The second term expresses the loss due to the absorption

of the wave when it passes through the shielding material. Dependence of SE on dielectric properties and magnetic properties can be expressed as

$$SE_R (dB) \approx 10 \log(\sigma_{ac}/(16\omega\epsilon_0\mu_r)) \quad (7)$$

and

$$SE_A (dB) = 20 \left\{ \frac{t}{\delta} \right\} \log e = 20 t \sqrt{\frac{\mu_r \omega \sigma_{ac}}{2}} = 8.68 \left(\frac{t}{\delta} \right) \quad (8)$$

where σ_{ac} depends on the dielectric properties ($\sigma_{ac} = \omega \epsilon_0 \epsilon''$) of the material, ω is the angular frequency ($\omega = 2\pi f$), ϵ_0 is the free space permittivity, and μ_r is the relative magnetic permeability of the sample.

Equation 7 and 8 reveal that with the increase in frequency, the SE_R value decreases while the contribution of SE_A increases. Reflection loss (SE_R) is the result of interaction of conducting particles in the conducting material and electromagnetic field and it has a relationship with the value of (σ_{ac}/μ_r) , which shows that for the larger conductivity of the material and smaller magnetic permeability there will be larger reflection loss. On the other hand, absorption loss, (SE_A) is caused by the heat loss under the action between electric dipole and /or magnetic dipole in the shielding material and the electromagnetic field so that the absorption loss is a function of the product $\sigma_{ac}\mu_r$. This indicates that for the higher absorption loss the material should not only have the higher electrical conductivity but also higher magnetic permeability.

It is convenient to express SE_R and SE_A in terms of the reflectance $-10 \log (1 - R)$ and effective absorbance $-10 \log (1 - A_{eff})$ in decibel (dB), respectively and can be expressed in the following equation⁴² as

$$SE_R = -10 \log(1 - R) \quad (9)$$

and

$$SE_A = -10 \log(1 - A_{eff}) = -10 \log\left(\frac{T}{1-R}\right) \quad (10)$$

For a material, the skin depth (δ) is the distance up to which the intensity of the electromagnetic wave decreases to $1/e$ of its original strength. The skin depth is related to angular frequency, relative permeability and total conductivity $\sigma_T = \sigma_{dc} + \sigma_{ac}$.

Fig. 6(a) shows the variation of total SE with frequency for different thickness samples while Fig. 6(b) shows SE_A and SE_R with frequency for barium ferrite decorated reduced graphene oxide composite at a thickness of 1, 1.5, 2, 2.5 and 3 mm in the frequency range of 12.4 -18 GHz (Ku-band). The graph depicts that the value of total SE and SE_A increases with the thickness of the sample which is in accordance with the shielding theory. On the other hand SE_R remains constant with increase in thickness in the whole frequency range. A value of 32 dB (SE_T) was achieved at a critical thickness of 3 mm. This value is higher as compared to shield prepared using reduced graphene oxide and as synthesized barium ferrite at 3 mm thickness as shown in Fig S2 (see supplementary information). A shield of thickness ~ 3 mm is sufficient to provide the SE greater than the limit (30 dB) required for techno-commercial applications as shown in Fig. 6(d). For the as-synthesized barium ferrite decorated reduced graphene oxide composite, the total SE is conquered by the absorption (27 dB) while the SE due to reflection (5 dB) contributes partially. Earlier reports on the EMI shielding and microwave absorption show that EMI SE increase linearly with the increase in thickness. The as synthesized barium ferrite decorated reduced graphene oxide composite shows absorption efficiency more than 99.8% (Fig. 6(c)) which means most of the EM energy incident on the shield attenuates and dissipated in the form of heat energy.

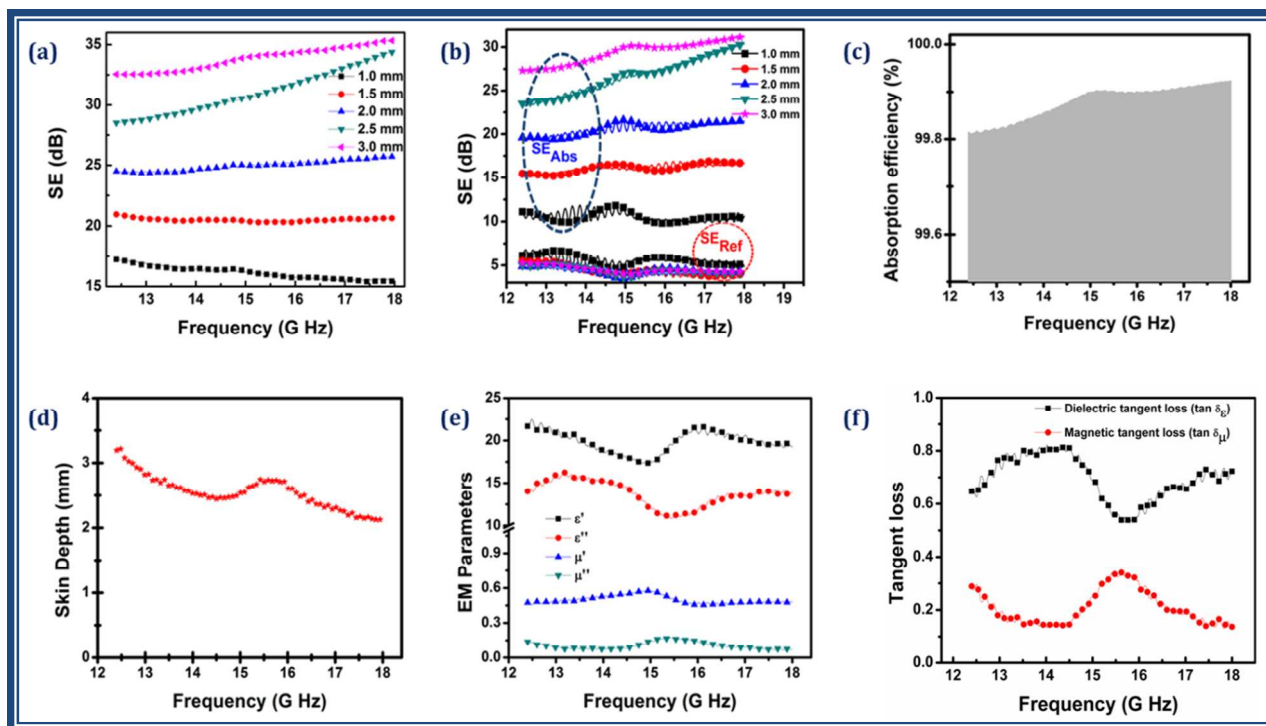


Fig. 6 Variation in EMI shielding effectiveness (a) SE_T (b) SE_A and SE_R with frequency for different thickness of BaFe₁₂O₁₉@RGO nanocomposite, (c) variation in absorption efficiency and (d) change in skin depth of BaFe₁₂O₁₉@RGO with the increase in frequency, frequency dependence of (e) real and imaginary parts of permittivity and permeability and (f) corresponding dielectric and magnetic tangent loss of BaFe₁₂O₁₉@RGO for a 3.0 mm thick sample.

The enhanced SE of the composite is a result of EM wave attenuation in the form of dielectric and magnetic losses. To elaborate more about the shielding performance of the barium ferrite decorated reduced graphene oxide composite complex permittivity and permeability of the composites were calculated using the observed S parameters. The real part $\epsilon'(\omega)$, $\mu'(\omega)$ of complex permittivity and permeability are mainly associated with the amount of polarization occurring in the material and symbolizes the storage ability of the electric and magnetic energy,

while the imaginary part $\epsilon''(\omega)$, $\mu''(\omega)$ accounts for dielectric and magnetic losses, respectively. The values of ϵ' are in the range of 22.5-17.3 meanwhile the values of ϵ'' are in the range of 15.3-10.8 in the frequency range of 12.4-18 GHz for barium ferrite decorated reduced graphene oxide composites as shown in Fig. 6(e). It is proposed that the barium ferrite decorated reduced graphene oxide composite show higher values of ϵ' and ϵ'' due to conducting reduced graphene oxide which may enhance the conductivity of the composite and electric polarization because the relative complex permittivity is a measure of the polarizability of a material which induces dipolar and electric polarization during the activation by an EM wave. The contribution to the space charge polarization appears due to the heterogeneity of the material. In heterogeneous dielectrics, the accumulation of virtual charges on the interface of two media having different dielectric constant, ϵ_1' and ϵ_2' and conductivities σ_1 and σ_2 respectively, lead to interfacial polarization and is known as Maxwell-Wagner polarization⁴³. The ratio of the imaginary to the real part (ϵ''/ϵ') is the 'dissipation factor', which is represented by $\tan\delta$, where δ is called as "loss angle" denoting the angle between the voltage and the charging current. The observed $\tan \delta_E$ is always greater than 0.6 in the entire frequency range indicating that the dielectric loss occurs in all frequency ranges.

The values of μ' are in the range of 0.57 - 0.45, meanwhile, the values of μ'' are in the range of 0.17 - 0.06. Dielectric tangent loss ($\tan \delta_E = \epsilon''/\epsilon'$) and the magnetic tangent loss ($\tan \delta_M = \mu''/\mu'$) of barium ferrite decorated reduced graphene oxide composite are also calculated using the permittivity and permeability parameters of the samples and presented in Fig. 6 (f). The presence of high permeability material like barium ferrite lowers the $\epsilon'(\omega)$ and enhances the impedance matching by improving the equality of $\epsilon'(\omega) = \mu'(\omega)$ which is a necessary condition for maximum attenuation of EM wave.

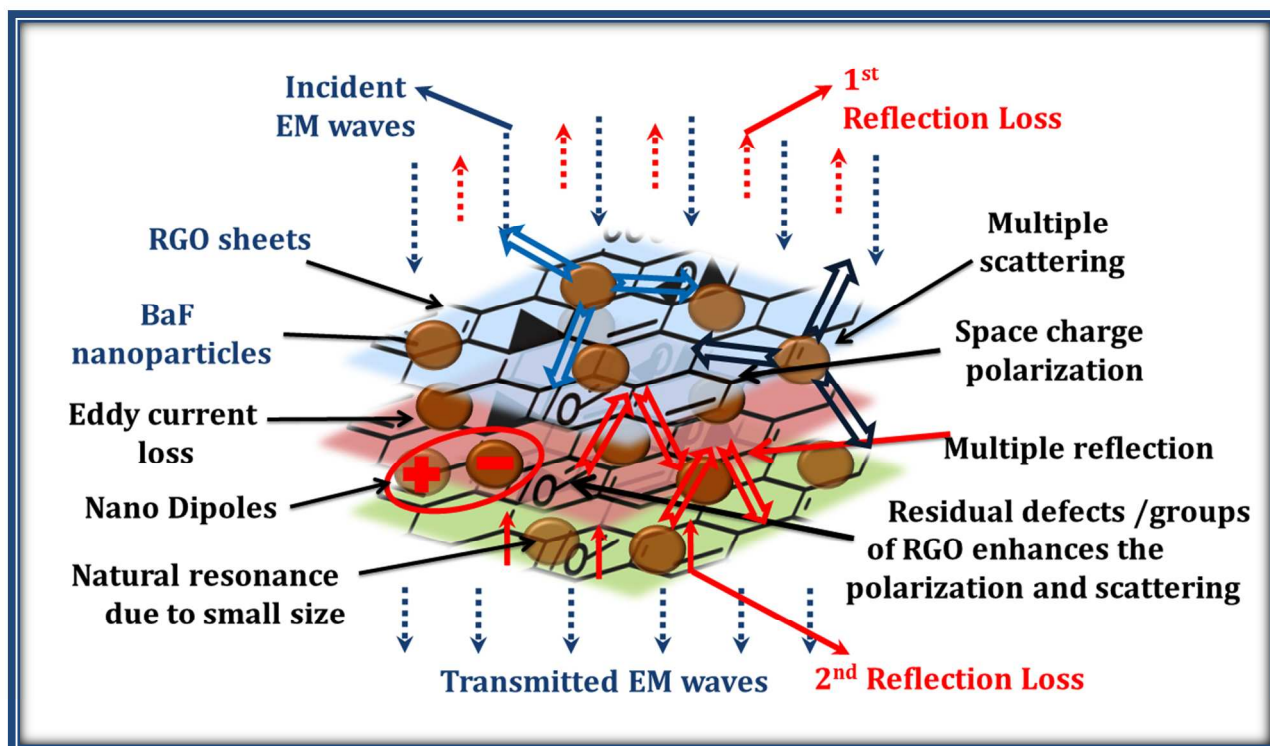


Fig. 7 Schematic representation of the proposed EMI shielding mechanism in $\text{BaFe}_{12}\text{O}_{19}@\text{RGO}$ nanocomposite

Notably, two humps were observed in $\tan \delta_E$ (shown in Fig. 6(f)) which proposed that the two main phenomena are responsible for dielectric losses. These may be interfacial polarization between RGO sheets and barium ferrite nanoparticles and high anisotropy energy of the nanocomposite. The high anisotropy energy may be ascribed to EM wave incident perpendicular to the RGO plane (as shown in Fig. 7).⁴⁴ Similarly, two humps observed in the $\tan \delta_M$ could be assigned to the natural resonances due to the small size effect of nanodimension barium ferrite and eddy currents during the activation by an EM field. These results suggest that barium ferrite decorated reduced graphene oxide composite has distinct dielectric and magnetic loss properties. Furthermore, the existence of residual defects/groups in RGO sheets and multiple reflections within the shield enhances the microwave shielding ability of the composites. A clear

demonstration of the shielding mechanism as discussed above is given in Fig.7. From all the above discussion, barium ferrite decorated reduced graphene oxide nanocomposite with minimal thickness 3 mm could be potentially applied for microwave shielding in radar frequency range. There is a further scope to study other two dimensional materials in place of RGO such as boron nitride nanosheets which has been found as a potential candidate for a variety of applications.⁴⁵⁻

46

Conclusion

In summary, barium ferrite decorated reduced graphene oxide nanocomposite has been successfully prepared using high energy ball milling. The structure and morphology of the as-synthesized nanocomposite were characterized by XRD, FTIR, VSM, Raman, SEM and TEM. The decoration of magnetic barium ferrite on the reduced graphene oxide sheets has been clearly seen in high resolution transmission electron microscopy. The total EMI shielding effectiveness of barium ferrite decorated graphene nanocomposite is achieved upto 32dB in Ku band frequency range (12.4-18 GHz). This value of shielding effectiveness crossed the limit of requirement for commercial applications and these nanocomposites are capable aspirants for making futuristic radar absorbers.

Acknowledgement

The authors wish to thank Dr. N. Vijayan and Dr. Vidyanand Singh for recording XRD pattern and HRTEM measurements of the sample, respectively.

References

1. D. D. L. Chung, *Carbon*, 2012, **50**, 3342-3353.

2. X. Sun, J. He, G. Li, J. Tang, T. Wang, Y. Guo and H. Xue, *Journal of Materials Chemistry C*, 2013, **1**, 765-777.
3. Z. Chen, C. Xu, C. Ma, W. Ren and H.-M. Cheng, *Advanced Materials*, 2013, **25**, 1296-1300.
4. A. P. Singh, M. Mishra, P. Sambyal, B. K. Gupta, B. P. Singh, A. Chandra and S. K. Dhawan, *Journal of Materials Chemistry A*, 2014, **2**, 3581-3593.
5. T. K. Gupta, B. P. Singh, V. N. Singh, S. Teotia, A. P. Singh, I. Elizabeth, S. R. Dhakate, S. K. Dhawan and R. B. Mathur, *Journal of Materials Chemistry A*, 2014, **2**, 4256-4263.
6. N. Li, Y. Huang, F. Du, X. He, X. Lin, H. Gao, Y. Ma, F. Li, Y. Chen and P. C. Eklund, *Nano Letters*, 2006, **6**, 1141-1145.
7. D. D. L. Chung, *Carbon*, 2001, **39**, 279-285.
8. D. D. L. Chung, *J. of Materi Eng and Perform*, 2000, **9**, 161-163.
9. S. Maiti, N. K. Shrivastava, S. Suin and B. B. Khatua, *ACS Applied Materials & Interfaces*, 2013, **5**, 4712-4724.
10. X. Li, H. Yi, J. Zhang, J. Feng, F. Li, D. Xue, H. Zhang, Y. Peng and N. Mellors, *J Nanopart Res*, 2013, **15**, 1-11.
11. K. Singh, A. Ohlan, V. H. Pham, B. R. S. Varshney, J. Jang, S. H. Hur, W. M. Choi, M. Kumar, S. K. Dhawan, B.-S. Kong and J. S. Chung, *Nanoscale*, 2013, **5**, 2411-2420.
12. Ramanathan T, A. A. Abdala, Stankovich S, D. A. Dikin, M. Herrera Alonso, R. D. Piner, D. H. Adamson, H. C. Schniepp, Chen X, R. S. Ruoff, S. T. Nguyen, I. A. Aksay, R. K. Prud'Homme and L. C. Brinson, *Nat Nano*, 2008, **3**, 327-331.
13. H. Wang, Q. Hao, X. Yang, L. Lu and X. Wang, *Nanoscale*, 2010, **2**, 2164-2170.
14. B. G. Choi, M. Yang, W. H. Hong, J. W. Choi and Y. S. Huh, *ACS Nano*, 2012, **6**, 4020-4028.
15. C. Berger, Z. Song, T. Li, X. Li, A. Y. Ogbazghi, R. Feng, Z. Dai, A. N. Marchenkov, E. H. Conrad, P. N. First and W. A. de Heer, *The Journal of Physical Chemistry B*, 2004, **108**, 19912-19916.
16. H. Gwon, H.-S. Kim, K. U. Lee, D.-H. Seo, Y. C. Park, Y.-S. Lee, B. T. Ahn and K. Kang, *Energy & Environmental Science*, 2011, **4**, 1277-1283.
17. N. Li, M. Zheng, H. Lu, Z. Hu, C. Shen, X. Chang, G. Ji, J. Cao and Y. Shi, *Chemical Communications*, 2012, **48**, 4106-4108.
18. Y. Liu, X. Dong and P. Chen, *Chemical Society Reviews*, 2012, **41**, 2283-2307.
19. Z. Huang, B. Chi, J. Guan and Y. Liu, *RSC Advances*, 2014, **4**, 18645-18651.
20. H. Zhao, Y. Du, L. Kang, P. Xu, L. Du, Z. Sun and X. Han, *CrystEngComm*, 2013, **15**, 808-815.
21. X. Liu, J. Wang, J. Ding, M. S. Chen and Z. X. Shen, *Journal of Materials Chemistry*, 2000, **10**, 1745-1749.
22. Y. Li, R. Yi, A. Yan, L. Deng, K. Zhou and X. Liu, *Solid State Sciences*, 2009, **11**, 1319-1324.
23. Y. Wang, Y. Huang, Q. Wang, Q. He and M. Zong, *Journal of Sol-Gel Science and Technology*, 2013, **67**, 344-350.
24. A. Ohlan, K. Singh, A. Chandra and S. K. Dhawan, *ACS Applied Materials & Interfaces*, 2010, **2**, 927-933.
25. A. Ohlan, K. Singh, A. Chandra and S. K. Dhawan, *Journal of Applied Polymer Science*, 2008, **108**, 2218-2225.
26. A. Ohlan, K. Singh, A. Chandra and S. K. Dhawan, *Applied Physics Letters*, 2008, **93**, -.

27. F. Xu, L. Ma, M. Gan, J. Tang, Z. Li, J. Zheng, J. Zhang, S. Xie, H. Yin, X. Shen, J. Hu and F. Zhang, *Journal of Alloys and Compounds*, 2014, **593**, 24-29.
28. P. Xu, X. Han, C. Wang, H. Zhao, J. Wang, X. Wang and B. Zhang, *The Journal of Physical Chemistry B*, 2008, **112**, 2775-2781.
29. D. C. Marcano, D. V. Kosynkin, J. M. Berlin, A. Sinitskii, Z. Sun, A. Slesarev, L. B. Alemany, W. Lu and J. M. Tour, *ACS Nano*, 2010, **4**, 4806-4814.
30. A. P. Singh, B. K. Gupta, M. Mishra, Govind, A. Chandra, R. B. Mathur and S. K. Dhawan, *Carbon*, 2013, **56**, 86-96.
31. W.-L. Song, J. Wang, L.-Z. Fan, Y. Li, C.-Y. Wang and M.-S. Cao, *ACS Applied Materials & Interfaces*, 2014.
32. A. P. Singh, M. Mishra, A. Chandra and S. K. Dhawan, *Nanotechnology*, 2011, **22**, 465701.
33. A. Nicolson and G. Ross, *Instrumentation and Measurement, IEEE Transactions on*, 1970, **19**, 377-382.
34. P. Sambyal, A. P. Singh, M. Verma, M. Farukh, B. P. Singh and S. K. Dhawan, *RSC Advances*, 2014, **4**, 12614-12624.
35. H. Zhang, D. Hines and D. L. Akins, *Dalton Transactions*, 2014, **43**, 2670-2675.
36. M. Naebe, J. Wang, A. Amini, H. Khayyam, N. Hameed, L. H. Li, Y. Chen and B. Fox, *Sci. Rep.*, 2014, **4**.
37. G. Wang, G. Chen, Z. Wei, X. Dong and M. Qi, *Materials Chemistry and Physics*, 2013, **141**, 997-1004.
38. V. Rane, S. Meena, S. Gokhale, S. M. Yusuf, G. Phatak and S. Date, *Journal of Elec Materi*, 2013, **42**, 761-768.
39. B. P. Singh, Prasanta, V. Choudhary, P. Saini, S. Pande, V. N. Singh and R. B. Mathur, *J Nanopart Res*, 2013, **15**, 1-12.
40. D.-X. Yan, P.-G. Ren, H. Pang, Q. Fu, M.-B. Yang and Z.-M. Li, *Journal of Materials Chemistry*, 2012, **22**, 18772-18774.
41. N. C. Das, D. Das, T. K. Khastgir and A. C. Chakraborty, *Composites A.*, 2000, **31**, 1069-1081.
42. N. F. Colaneri and L. Schacklette, *Instrumentation and Measurement, IEEE Transactions on*, 1992, **41**, 291-297.
43. J. Zhu, H. Gu, Z. Luo, N. Haldolaarachige, D. P. Young, S. Wei and Z. Guo, *Langmuir*, 2012, **28**, 10246-10255.
44. N. Yousefi, X. Sun, X. Lin, X. Shen, J. Jia, B. Zhang, B. Tang, M. Chan and J.-K. Kim, *Advanced Materials*, 2014, **26**, 5480-5487.
45. X. Song, J. Hu and H. Zeng, *Journal of Materials Chemistry C*, 2013, **1**, 2952-2969.
46. H. Zeng, C. Zhi, Z. Zhang, X. Wei, X. Wang, W. Guo, Y. Bando and D. Golberg, *Nano Letters*, 2010, **10**, 5049-5055.